Clustering effects and decay analysis of the light-mass $N = Z$ and $N \neq Z$ composite systems formed in heavy ion collisions

Manpreet Kaur,[1] BirBikram Singh,[1,*] S. K. Patra,[2] and Raj K. Gupta[3]
[1]*Department of Physics, Sri Guru Granth Sahib World University, Fatehgarh Sahib-140406, India*
[2]*Institute of Physics, Sachivalaya Marg, Bhubaneswar-751005, India*
[3]*Department of Physics, Panjab University, Chandigarh-160014, India*
(Received 20 September 2016; revised manuscript received 19 November 2016; published 26 January 2017)

We investigate the clustering effects in light mass $N = Z$ and $N \neq Z$ composite systems ^{20}Ne*, ^{28}Si*, ^{40}Ca* and ^{21,22}Ne*, ^{39}K*, respectively, formed in low-energy heavy ion reactions at different excitation energies, within the collective clusterization approach of the dynamical cluster-decay model (DCM) of Gupta and collaborators based on quantum-mechanical fragmentation theory (QMFT). Considering quadrupole deformed and compact orientated nuclei, a comparative decay analysis of these systems has been undertaken for the emission of different intermediate mass fragments (IMFs) or clusters, specifically the IMFs having $Z = 3$, 4, and 5 (or $Z = 7$, 6, and 5 complimentary fragments from the ^{20}Ne* and ^{21,22}Ne* composite systems) which are having the experimental data available for their Z distribution. Quite interestingly, the QMFT supports clustering in $N = Z$ (^{20}Ne* and ^{28}Si*) and $N \neq Z$ (^{21}Ne* and ^{22}Ne*) nuclear systems at excitation energies corresponding to their respective decay threshold or resonant-state energies for the 4α, ^{16}O cluster and non-α cluster ^{14}C (more so in ^{22}Ne* $N \neq Z$ composite system), supported by the Ikeda diagrams, taking into account the proper pairing strength in the temperature-dependent liquid drop energies. Within the DCM, we notice that at higher excitation energies in addition to $x\alpha$-type (where x is an integer) clusters from $N = Z$ composite systems and xn-$x\alpha$-type clusters from $N \neq Z$ composite systems, np-$x\alpha$-type clusters are relatively quite dominant, with larger preformation probability due to the decreased pairing strength at higher temperatures in the liquid drop energies. Also, the study reveals the presence of competing reaction mechanisms of compound nucleus (fusion-fission, FF) and of noncompound nucleus origin (deep inelastic orbiting, DIO) in the decay of very-light-mass composite systems ^{20,21,22}Ne* and ^{28}Si* at different excitation energies. The DIO contribution in the IMF cross section $\sigma_{\rm IMF}$ is extracted for these composite systems, $\sigma_{\rm IMF}$ is given as the sum of FF cross section $\sigma_{\rm FF}$ and DIO cross section $\sigma_{\rm DIO}$. The DCM calculated FF cross sections $\sigma_{\rm FF}^{\rm DCM}$ are in good agreement with the available experimental data.

DOI: 10.1103/PhysRevC.95.014611

I. INTRODUCTION

An atomic nucleus remains the center of very exciting field of research, with many interesting questions still unanswered. Nuclear physics being even one of the very successful disciplines for almost one century, still looking forward to so many challenges on theoretical as well as experimental fronts. One of the biggest challenges is the nucleon-nucleon interaction inside the nucleus, which is not precisely known as yet. Furthermore, on one hand too many particles to deal with quantum mechanically and on the other hand, too few particles to be treated statistically in an accurate way, makes the matter more challenging. Theoretical physicists are expected to be further brave for such facts with the upcoming fast computational facilities and experimentalists are looking for their data to be explained with nuclear models.

Nuclear cluster models are complementing other models in the field, to explain successfully a number of nuclear phenomena. According to the cluster models, these phenomena could be understood keeping in view the fact that nucleons lumped together into a cluster, for further interactions among various nucleon clusters, rather than as free nucleons. The tightly bound alpha particle (^{4}He) with protons and neutrons, two each, makes a very special case of nuclear clustering due to its much larger binding energy than that of other light nuclei. In 1928, Gamow explained very well the spontaneous formation of an alpha particle before its tunneling through the potential barrier, while understanding the alpha decay of trans-lead elements [1]. The most famous Hoyle state of ^{12}C, constituted of three alpha clusters, was predicted in 1953 [2] to account for the abundance of carbon in the universe and subsequently measured in 1957 [3]. Since then a number of ideas have been explored to study the structure of various alpha conjugate nuclei ($x\alpha$, where x is integer) or $N = Z$ nuclei from ^{12}C to ^{40}Ca [4]. These studies, specifically the Ikeda diagrams, portray that these nuclei can be viewed as a combination of alpha clusters or alpha plus heavier alpha conjugate clusters depending on their excitation energy.

It is further being explored to understand the structure of non-alpha conjugate nuclei (with added neutrons to alpha conjugate nuclei) or $N \neq Z$ nuclei within the above picture. The neutron-rich $N \neq Z$ nuclei are visualized in terms of covalent exchanging of valence neutrons between the α cores and by this way nuclear systems surmount the difficulty of maximizing the interaction of valence or excess neutron with the α-core nucleons [5]. The cluster structures are also predicted in the case of $N = Z$ and $N \neq Z$ nuclei from ^{16}O to ^{40}Ca. The cluster states are probed experimentally through the quasi-elastic scattering, transfer or the cluster

*birbikramsingh@sggswu.edu.in

knockout reactions and electromagnetic transitions [6]. The cluster structures have been studied experimentally in isotopes of Be and B, ^{18}O, ^{20,21,22}Ne, ^{24}Mg, ^{28}Si, ^{32}S, ^{40}Ca [7,8]. Moreover, experimentally, Rogachev *et al.* [7] have worked out successfully on the prediction of $\alpha + np + \alpha$ clustering for $N \neq Z$, ^{10}B nucleus.

Many more theoretical attempts have been made to explain the clustering in such light nuclei. Two of us (S.K.P. and R.K.G.) have studied [9] the clustering in light, stable, and exotic nuclei within the relativistic mean-field approach which explains the well established cluster structures in both the ground and intrinsic excited states of these nuclei. In this study, α clustering and halo structures have also been explored for the $^{6-14}$Be and ^{11,13,15,17,19}B isotopes, respectively, having $\alpha + \alpha + xn$ structures with $\alpha + \alpha$ as the core and $\alpha + \alpha + \mathrm{p} + xn$ structures with $\alpha + \alpha + p$ as the core. Along the same lines, Ebran *et al.* have studied [10] the clustering in light $N = Z$, ^{20}Ne nucleus within the density functional theory and explored that the cause of cluster formation lies in the effective nuclear interaction. Also, one of us (R.K.G.) and collaborators have explored [11] the clustering prospects in light neutron-rich ^{18,20}O and ^{22}Ne in the resonant excited states within quantum-mechanical fragmentation theory (QMFT), by taking into account the proper temperature-dependent pairing strength [$\delta(T)$] in the temperature-dependent liquid drop energy. The results support the possibility of ^{14}C ($3\alpha + 2n$) clustering, in addition to α clustering in these nuclei, which supports the predictions of extended Ikeda diagram [5] for n-rich nuclei.

Low-energy heavy ion collisions provide a wonderful probe to analyze the cluster structure in the decay of composite systems formed in these reactions. The decay products of the very-light-mass composite systems (A $\sim$ 20–40) have been analyzed extensively, including $N = Z$ as well as $N \neq Z$ composite systems [12–14]. The structure of nucleus also plays an important role in fragment or cluster emission. A lot of effort has been made to study the effect of clustering on the reaction mechanism of light $N = Z$ composite nuclear systems, i.e., $^{16}\mathrm{O} + ^{12}\mathrm{C}$ [15], $^{20}\mathrm{Ne} + ^{12}\mathrm{C}$ [16], $^{24}\mathrm{Mg} + ^{12}\mathrm{C}$ [17], and $^{28}\mathrm{Si} + ^{12}\mathrm{C}$ [18] reactions. In these cases, in addition to the fusion-fission (FF) path of decay from equilibrated compound nuclei (CN), the projectile and target nuclei have another possibility to form a dinuclear composite with subsequent emission of intermediate mass fragments (IMFs) or clusters prior to equilibration; also referred to as deep inelastic orbiting (DIO). Thus, observed fragments or clusters may result either from the decay of equilibrated CN or from DIO prior to the formation of CN. The competition between the two decay processes is also interpreted in terms of number of open channels (NOC) available for the decay [19]. Large NOC indicates that FF process dominates with regard to the faster process of DIO with the memory of entrance channel. In the light-mass region, the systems studied having small NOC are $^{16}\mathrm{O} + ^{12}\mathrm{C}$ [15], $^{20}\mathrm{Ne} + ^{12}\mathrm{C}$ [16], $^{24}\mathrm{Mg} + ^{12}\mathrm{C}$ [17], and $^{28}\mathrm{Si} + ^{12}\mathrm{C}$ [18], and the systems studied having large NOC include $^{10,11}\mathrm{B} + ^{16,17,18}\mathrm{O}$, $^{31}\mathrm{P} + ^{16}\mathrm{O}$, $^{35}\mathrm{Cl} + ^{12}\mathrm{C}$, and $^{36}\mathrm{Ar} + ^{12}\mathrm{C}$ [20–22], which have also been studied successfully within QMFT-based dynamical cluster-decay model (DCM) [23] showing competing decay modes for the system ($^{20}\mathrm{Ne} + ^{12}\mathrm{C}$) with the smaller value of NOC and the only decay mode, i.e., fusion-fission for the systems $^{31}\mathrm{P} + ^{16}\mathrm{O}$ and $^{19}\mathrm{F} + ^{12}\mathrm{C}$ having large NOC values.

It is also relevant to note here that one of us (R.K.G.) and others have studied [24] the clustering effects in case of $N = Z$ and $N \neq Z$ composite systems formed in the heavy ion transfer collisions, within the QMFT. The study reveals that, in case of $N = Z$, $A = 4x$ colliding nuclei, the minima in the potential-energy surface (PES) lie only at α-particle-like nuclei whereas, upon adding the neutrons to either the projectile or target or both, the colliding nuclei (i.e., $N \neq Z$ nuclei) lead gradually to the disappearance or decrease in the depth of minima at α clusters along with the appearance of minima at non-α clusters. This well-established collective clusterization approach of the DCM may also be further explored to study the cluster structure of light-mass $N = Z$ and $N \neq Z$ composite nuclei formed in the heavy ion collision reactions.

Recall that the DCM has been applied successfully to study the decay of the light-mass compound systems ^{28}Al*, ^{31}P*, ^{32}S*, ^{39}K*, ^{40}Ca*, ^{48}Cr*, and ^{56}Ni* [23,25–27]. Also, the DCM explains successfully the fragment emission or decay characteristics of medium, heavy, and superheavy compound systems. Within the DCM, the decay of a compound system is studied as collective clusterization process for the emission of light particles LPs, IMFs, heavy-mass fragments (HMFs), and FF fragments while the statistical models treats the emission of different processes on different footings for different mass regions. The DCM incorporates the nuclear structure effects through preformation probability P_0 of different clusters in the decaying composite system, an information missing in the statistical models. The DCM is an extended version of the preformed cluster model (PCM) of Gupta and collaborators to study the excited-state decay of compound systems. The cluster radioactivity, the manifestation of clustering in the nuclei, has been studied successfully within the formalism of the PCM [28]. Within the PCM, the cluster emission of mass varying from ^{12}C to ^{34}Si in cluster radioactive decay process of nuclei in the trans-lead mass region, have been examined with inclusion of quadrupole and higher-order deformations and noncompact orientations.

In the present work, within the QMFT, we have investigated for α clustering in light-mass $N = Z$ and $N \neq Z$ nuclear systems ^{20}Ne*, ^{28}Si*, and ^{21,22}Ne*, respectively, in their intrinsic excited state at resonant-state energies corresponding to 4α, ^{16}O cluster, and non-α cluster ^{14}C (from ^{22}Ne* $N \neq Z$ composite system only), given by the Ikeda diagrams. It may be pointed out here that we have confined ourselves to the resonant-state energies of these nuclear systems, corresponding to ^{16}O and ^{14}C (from ^{22}Ne*) clusters, only to explore the effect of pairing strength in the liquid drop energies upon clustering. As we will see in the following, with respect to the higher excitation energies for these composite systems, clustering effects get changed due to smaller pairing strength in the liquid drop energy. Thus, the decay analysis of the above composite systems formed in low-energy heavy ion reactions at different excitation energies has been carried out within the DCM.

The experimental data [12–14] for the excited composite systems ^{20,21,22}Ne*, ^{28}Si*, ^{39}K*, and ^{40}Ca* formed in the

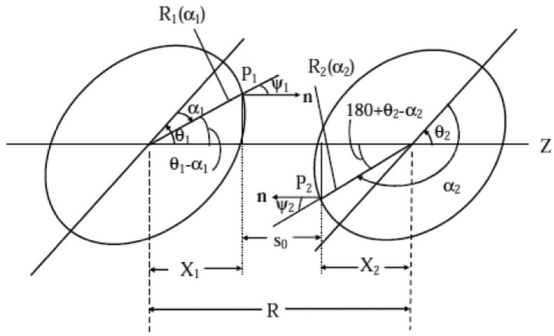

FIG. 1. Schematic configuration of two equal or unequal axially symmetric deformed, oriented nuclei, lying in the same plane (azimuthal angle $\phi = 0^\circ$) for various θ_1 and θ_2 values in the range 0° to 180°. The θ_i are measured anticlockwise from the collision axis and angle α_i clockwise from the symmetry axis.

reactions ^{10,11}B + ^{10,11}B, ^{16}O + ^{12}C, ^{11}B + ^{28}Si, ^{12}C + ^{27}Al, and ^{12}C + ^{28}Si, respectively, at different excitation energies is available for the emission of IMFs having $Z = 3$, 4, and 5 (or $Z = 7$, 6, and 5 complimentary fragments for the ^{20}Ne* and ^{21,22}Ne* composite systems) with their Z-distribution data. It is relevant to mention here that the decay of extremely-light-mass systems ^{20,21,22}Ne* formed in reactions ^{10,11}B + ^{10,11}B has been studied earlier [29] within the DCM for the binary symmetric decay (BSD) only at $E_{\rm lab} = 48$ MeV. We found that the FF is in competition with DIO for the BSD and that, with the inclusion of quadrupole deformation and orientation effects, the contribution of the FF process increases in ^{20}Ne* in comparison with ^{21,22}Ne*. The decay of ^{39}K* and ^{40}Ca* composite systems have also been studied earlier within the DCM, but for spherical consideration of nuclei [25].

In the following, a comparative decay analysis of the light-mass $N = Z$ (^{20}Ne*, ^{28}Si*, ^{40}Ca*) and $N \neq Z$ (^{21,22}Ne*, ^{39}K*) composite systems has been made within the DCM, at different excitation energies, where experimental data are available for the IMFs. The competitive decay modes of DIO in the yields of measured IMFs have been evaluated empirically, for the light composite systems under study, since we focus here mainly on the clustering effects in the equilibrated composite systems in the form of FF contribution in the yields of IMFs. The calculations of the DIO process will be taken up in future studies. Also, it is important to understand how the FF process evolves with increasing energies. It is quite important to explore and compare the clustering effects in these $N = Z$ α conjugate and $N \neq Z$ non-α conjugate composite systems as these have also been studied experimentally and are widely in need of a more theoretical interpretation.

Section II presents in brief the QMFT-based collective clusterization approach of the DCM, where the deformation effects are included up to quadrupole deformations (β_{2i}) with "compact orientations" (θ_i, $i = 1,2$), for the case of coplanar nuclei (azimuthal angle $\phi = 0^\circ$), shown schematically in Fig. 1 (see also Table 1 of Ref. [30]), and obtained as in Ref. [31] for the hot fusion process. The calculations and results are discussed in Sec. III. Finally, the conclusions are given in Sec. IV.

II. THE DYNAMICAL CLUSTER-DECAY MODEL

The DCM, based on QMFT [32–34], is used to study the decay of hot and rotating compound systems formed in heavy ion reactions and is an extended version of the PCM, as already mentioned in the introduction. It involves the two-step process of cluster preformation followed by the penetration through the interaction barrier, analogous to the α decay where preformation was taken to be unity. It is worked out in terms of (i) the collective coordinate of mass (and charge) asymmetry $\eta = (A_1 - A_2)/(A_1 + A_2)$ [and $\eta_Z = (Z_1 - Z_2)/(Z_1 + Z_2)$] and (ii) relative separation R, (iii) multiple deformations β_{λ_i}, $\lambda = 2$, 3, 4, and (iv) orientations θ_i of two nuclei in the same plane. These coordinates η and R, respectively, characterize the nucleon division (or exchange) between outgoing fragments and the transfer of kinetic energy of incident channel ($E_{\rm c.m.}$) to internal excitation [total excitation (TXE) or total kinetic energy (TKE)] of the outgoing channel. The TKE and TXE of fragments is related to CN excitation energy as $E^*_{\rm CN} + Q_{\rm out}(T) = {\rm TKE}(T) + {\rm TXE}(T)$.

The decay cross section of equilibrated CN, using the decoupled approximation of R and η motions, is defined in terms of ℓ partial waves as [35,36]

$$\sigma = \frac{\pi}{k^2}\sum_{\ell=0}^{\ell_c}(2\ell+1)P_0P, \quad k = \sqrt{\frac{2\mu E_{\rm c.m.}}{\hbar^2}}, \tag{1}$$

where the preformation probability P_0 and the penetrability P refers to η and R motion, respectively, and ℓ_c is the critical angular momentum:

$$\ell_c = R_a\sqrt{2\mu[E_{\rm c.m.} - V(R_a,\eta_{in},\ell=0)]}/\hbar.$$

R_a is the first turning point, defined later, where the penetration starts. The structure effects of the CN, a distinct advantage of the DCM over the statistical models, enters the model via the preformation probabilities P_0 of the fragments. In case, the noncompound nucleus (nCN) component, i.e., DIO, were not measured in the yield of IMF, it can be estimated empirically, $\sigma_{\rm DIO} = \sigma^{\rm Expt}_{\rm IMF} - \sigma^{\rm DCM}_{\rm FF}$, where $\sigma_{\rm DIO}$, $\sigma^{\rm Expt}_{\rm IMF}$, and $\sigma^{\rm DCM}_{\rm FF}$ are, respectively, the DIO, experimental IMF, and DCM-calculated FF cross sections.

The P_0 is given by the solution of stationary Schrödinger equation in η, at a fixed $R = R_a$,

$$\left\{-\frac{\hbar^2}{2\sqrt{B}_{\eta\eta}}\frac{\partial}{\partial\eta}\frac{1}{\sqrt{B}_{\eta\eta}}\frac{\partial}{\partial\eta} + V_R(\eta,T)\right\}\psi^\nu(\eta) = E^\nu\psi^\nu(\eta), \tag{2}$$

with $\nu = 0,1,2,3,\ldots$ referring to ground-state ($\nu = 0$) and excited-state solutions summed over as a Boltzmann-like function

$$|\psi|^2 = \sum_{\nu=0}^{\infty}|\psi^\nu|^2\exp(-E^\nu/T). \tag{3}$$

Then, the probability of cluster preformation is

$$P_0(A_i) = |\psi(\eta(A_i))|^2 \frac{2}{A^*_{\rm CN}} \sqrt{B_{\eta\eta}}, \tag{4}$$

where $i = 1$ or 2 and $B_{\eta\eta}$ are the smooth hydrodynamical mass parameters [37].

For clustering effects in nuclei we look for the maxima in $P_0(A_i)$ (as shown in Fig. 2) or the energetically favored potential-energy minima in the fragmentation potential $V_R(\eta,T)$. $V_R(\eta,T)$ in Eq. (2), for fixed β_{λ_i}, is the potential energy for all possible mass combinations A_i, corresponding to the given charges Z_i minimized for each mass fragmentation coordinate η. The fragmentation potential is defined as

$$\begin{aligned} V_R(\eta,T) = &\sum_{i=1}^{2} [V_{\rm LDM}(A_i,Z_i,T)] + \sum_{i=1}^{2} [\delta U_i] \exp\left(-\frac{T^2}{T_0^2}\right) \\ &+ V_c(R,Z_i,\beta_{\lambda_i},\theta_i,T) + V_P(R,A_i,\beta_{\lambda_i},\theta_i,T) \\ &+ V_\ell(R,A_i,\beta_{\lambda_i},\theta_i,T), \end{aligned} \tag{5}$$

where V_c, V_p, V_l are temperature-dependent Coulomb, nuclear proximity, and angular-momentum-dependent potentials for deformed and oriented nuclei. $B_i = V_{\rm LDM}(A_i,Z_i,T) + \delta U_i$, $i = 1,2$, are the binding energies of two nuclei, where δU are the "empirical" shell corrections, i.e., the microscopic part [38] of the binding energy, and $V_{\rm LDM}$ is the liquid drop energy, i.e.,

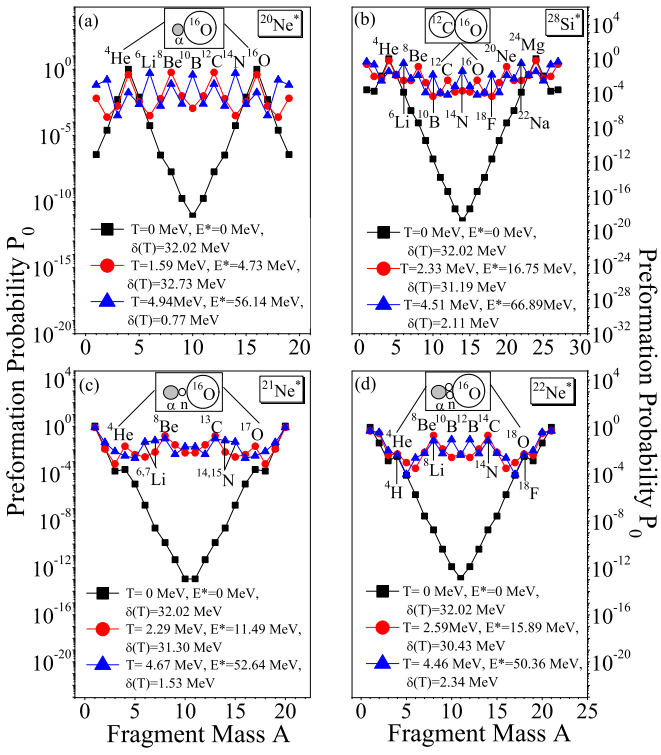

FIG. 2. Variation of the preformation probability P_0 with fragment or cluster mass (A_i, $i = 1,2$) for the decay of $N = Z$ or α conjugate systems (a) ^{20}Ne* and (b) ^{28}Si*, and $N \neq Z$ or non-α conjugate systems (c) ^{21}Ne* and (d) ^{22}Ne*, at T values of their corresponding excited resonant states and the experimentally available excited state [13].

the macroscopic part. The T-dependent liquid drop part of the binding energy $V_{\rm LDM}(T)$ is taken from Davidson *et al.* [39], based on the semi-empirical mass formula of Seeger [40], as

$$\begin{aligned} V_{\rm LDM}(A,Z,T) = &\alpha(T)A + \beta(T)A^{\frac{2}{3}} \\ &+ \left(\gamma(T) - \frac{\eta(T)}{A^{\frac{1}{3}}}\right)\left(\frac{I^2 + 2|I|}{A}\right) \\ &+ \frac{Z^2}{R_0(T)A^{\frac{1}{3}}}\left(1 - \frac{0.7636}{Z^{\frac{2}{3}}} - \frac{2.29}{[R_0(T)A^{\frac{1}{3}}]^2}\right) \\ &+ \delta(T)\frac{f(Z,A)}{A^{\frac{3}{4}}}, \end{aligned} \tag{6}$$

where

$$I = a_a(Z - N), \quad a_a = 1.0, \tag{7}$$

and $f(Z,A) = (-1,0,1)$, for even-even, even-odd, and odd-odd nuclei, respectively. The temperature-dependent binding energies are obtained from Ref. [39] with its constants at $T = 0$ refitted [35,36] to give the ground state ($T = 0$) experimental binding energies [41] and, where the data are not available, the theoretical binding energies are taken from Ref. [42]. It is important to point out here that one of us (R.K.G.) and co-workers have shown [11,43] that for both the α-nucleus and ^{14}C clustering in nuclei, a modified temperature dependence of the pairing energy coefficient $\delta(T)$ is essential in the temperature-dependent liquid drop energy (refer to Fig. 3 of Ref. [11]). In the following, we have further highlighted the significance of an appropriate $\delta(T)$ in the present calculations while comparing the clustering effects in the $N = Z$, ^{20}Ne*, ^{28}Si* (or α conjugate) and $N \neq Z$, ^{21,22}Ne* (or non-α conjugate) nuclear systems (refer to Fig. 2, discussed in detail in the next section).

The Coulomb potential V_c for deformed and oriented nuclei is defined as

$$\begin{aligned} &V_c(R,Z_i,\beta_{\lambda_i},\theta_i,T) \\ &= Z_1Z_2e^2/R(T) + 3Z_1Z_2e^2 \sum_{\lambda,i=1,2} \frac{R_i^\lambda(\alpha_i,T)}{(2\lambda+1)R^{\lambda+1}} \\ &\times Y_\lambda^{(0)}(\theta_i)\left[\beta_{\lambda_i} + \frac{4}{7}\beta_{\lambda_i}^2 Y_\lambda^{(0)}(\theta_i)\right]. \end{aligned} \tag{8}$$

The deformation parameters β_{λ_i} of the nuclei are taken from the tables of Möller *et al.* [42], and the orientations θ_i are the "optimum" [30] or "compact" orientations [31] of the "hot" fusion process.

The nuclear proximity potential

$$V_p(s_0(T)) = 4\pi\,\bar{R}(T)\gamma b(T)\Phi(s_0(T)), \tag{9}$$

where γ, the nuclear surface energy constant, is given by

$$\gamma = 0.9517\left[1 - 1.7826\left(\frac{N-Z}{A}\right)^2\right] \text{MeV/fm}^2, \tag{10}$$

and $b(T) = 0.99(1 + 0.009T^2)$ is the nuclear surface thickness and $\bar{R}(T)$ is the root mean square radius of the Gaussian curvature and $\Phi(s_0(T))$ is the universal function, independent of the geometry of the system but dependent on the minimum

separation distance $s_0(T)$ depicted in Fig. 1, as

$$\Phi(s_0(T)) = \begin{cases} -\frac{1}{2}(s_0-2.54)^2 - 0.0852(s_0-2.54)^3, & s_0 \leqslant 1.2511 \\ -3.437\exp\left(-\frac{s_0}{0.75}\right), & s_0 \geqslant 1.2511. \end{cases} \quad (11)$$

The minimum distance s_0, for a fixed R, is defined (see Fig. 1) as

$$s_0 = R - X_1 - X_2 = R - R_1(\alpha_1)\cos(\theta_1 - \alpha_1) - R_2(\alpha_2)\cos(180^\circ + \theta_2 - \alpha_2), \quad (12)$$

where, for s_0 to be minimum, the conditions on s_0 are [44]

$$\frac{\partial s_0}{\partial \alpha_1} = \frac{\partial s_0}{\partial \alpha_2} = 0, \quad (13)$$

resulting in

$$\tan(\theta_1 - \alpha_1) = -R_1^{'}(\alpha_1)/R_1(\alpha_1), \quad (14)$$

$$\tan(180^\circ + \theta_2 - \alpha_2) = -R_2^{'}(\alpha_2)/R_2(\alpha_2). \quad (15)$$

Here, $R_i^{'}(\alpha_i)$ is the first-order derivative of $R_i(\alpha_i)$ with respect to α_i. Note that the above conditions refer to perpendiculars (normal vectors) at the points P_1 and P_2 in Fig. 1, and hence minimum s_0 defines the so-called optimum [30] or compact configuration [31], respectively, for small (positive or negative, including zero value) or large positive β_{4i}. Thus, $s_0(T)$ gives the minimum separation distance along the colliding Z axis between any two deformed, coplanar nuclei, denoted as the neck-length parameter $\Delta R(\eta, T)$ in the following [refer to Eq. (21)].

The angular-momentum-dependent potential is given by

$$V_\ell(T) = \frac{\hbar^2 \ell(\ell+1)}{2I(T)}, \quad (16)$$

where

$$I(T) = I_s(T) = \mu R^2 + \tfrac{2}{5}A_1 m {R_1}^2(\alpha_1, T) + \tfrac{2}{5}A_2 m {R_2}^2(\alpha_2, T) \quad (17)$$

is the moment of inertia for the sticking limit. This limit is defined for the separation distance ΔR to be within the range of nuclear proximity ($\sim$2 fm). The penetration probability P in Eq. (1) is calculated by using the Wenzel–Kramers–Brillouin (WKB) integral as

$$P = \exp\left[-\frac{2}{\hbar}\int_{R_a}^{R_b}\{2\mu[V(R) - Q_{\rm eff}]\}^{1/2} dR\right], \quad (18)$$

where $V(R)$ is the scattering potential at each R value, calculated as sum of Coulomb, proximity, and angular-momentum-dependent potential, with R_a and R_b as the first and second turning point, satisfying

$$V(R_a, \ell) = V(R_b, \ell) = Q_{\rm eff}(T, \ell). \quad (19)$$

The ℓ dependence of R_a is defined by

$$V(R_a, \ell) = Q_{\rm eff}(T, \ell = \ell_{\rm min}), \quad (20)$$

which means that R_a, given by equation above is the same for all ℓ values and that $V(R_a, \ell)$ acts like an (effective) Q value [$Q_{\rm eff}(\mathrm{T}, \ell)$] for the decay of a hot compound system. The $\ell_{\rm min}$ value refers to the minimum value that starts contributing to WKB integral. As the ℓ value increases, the $Q_{\rm eff}(T)$ value increases and hence $\mathrm{V}(R_a, \ell)$ increases (see Fig. 3). Equation (18) is solved analytically [45], as shown in Fig. 3 for the illustrative case of symmetric decay of $N = Z$ composite systems.

The first turning point R_a of the penetration path is given as

$$R_a = R_1(\alpha_1, T) + R_2(\alpha_2, T) + \Delta R(\eta, T), \quad (21)$$

with the radius vector $R_i(\alpha_i, T)$ defined as

$$R_i(\alpha_i, T) = R_{0i}(T)\left[1 + \sum_\lambda \beta_{\lambda_i} Y_\lambda^{(0)}(\alpha_i)\right], \quad (22)$$

where

$$R_{0i}(T) = \left[1.28A_i^{1/3} - 0.76 + 0.8A_i^{-1/3}\right](1 + 0.0007T^2), \quad (23)$$

with T calculated by using $E^*_{\rm CN} = (\frac{A}{8})T^2 - T$. The choice of parameter R_a, for a best fit to the data, allows us to relate in a simple way the $\mathrm{V}(R_a)$ to the top of the barrier V_B for each ℓ, by defining their difference $\Delta \mathrm{V}_B$ as the effective "lowering of the barrier":

$$\Delta V_B = V(R_a) - V_B.$$

Note that $\Delta \mathrm{V}_B$ is defined as a negative quantity because the barrier actually used is effectively lowered which is an inbuilt property of the DCM. This ensures that $V(R_a)$ $(= Q_{\rm eff})$ lies below the barrier, as illustrated in Fig. 3 for $\ell_{\rm min}$ and ℓ_c values. It shows that the magnitude of $\Delta \mathrm{V}_B$ decreases with increase in ℓ value.

III. CALCULATIONS AND DISCUSSION

In this section we first present the calculations and discussion within the QMFT, for the decay of light-mass $N = Z$ (^{20}Ne* and ^{28}Si*) and $N \neq Z$ (^{21}Ne* and ^{22}Ne*) nuclear systems with considerations of quadrupole deformations and "hot" compact orientations of nuclei. The calculations have been done at $T = 0$ as well as the corresponding excitation energies of the nuclear systems for their respective decay threshold or resonant-state energies for the 4α, i.e., ^{16}O cluster, except for the ^{22}Ne* system where the chosen threshold or resonant-state energy is for the ^{14}C cluster, given by the Ikeda diagram. Second, we present here the calculations and discussion within the QMFT-based DCM, for the decay of highly excited light-mass $N = Z$ (^{20}Ne*, ^{28}Si*, and ^{40}Ca*) and $N \neq Z$ (^{21}Ne*, ^{22}Ne*, and ^{39}K*) composite systems formed in heavy ion collisions. We intend to analyze the effects of the rising temperature on the clustering in these systems under study, specifically, ^{20}Ne*, ^{28}Si*, ^{21}Ne*, and ^{22}Ne* from ground state $T = 0$ to the corresponding resonant-state temperature (as mentioned above) and beyond at the higher excitation energies. At higher excitation energies, the available experimental data for the IMFs or clusters having $Z = 5,6,7$ (for ^{20}Ne*, ^{21}Ne*, ^{22}Ne*) and $Z = 3,4,5$ for ^{28}Si* will be compared with the DCM calculations.

It is quite important to explore and compare the clustering effects in these $N = Z$ or α conjugate and $N \neq Z$ or non-α

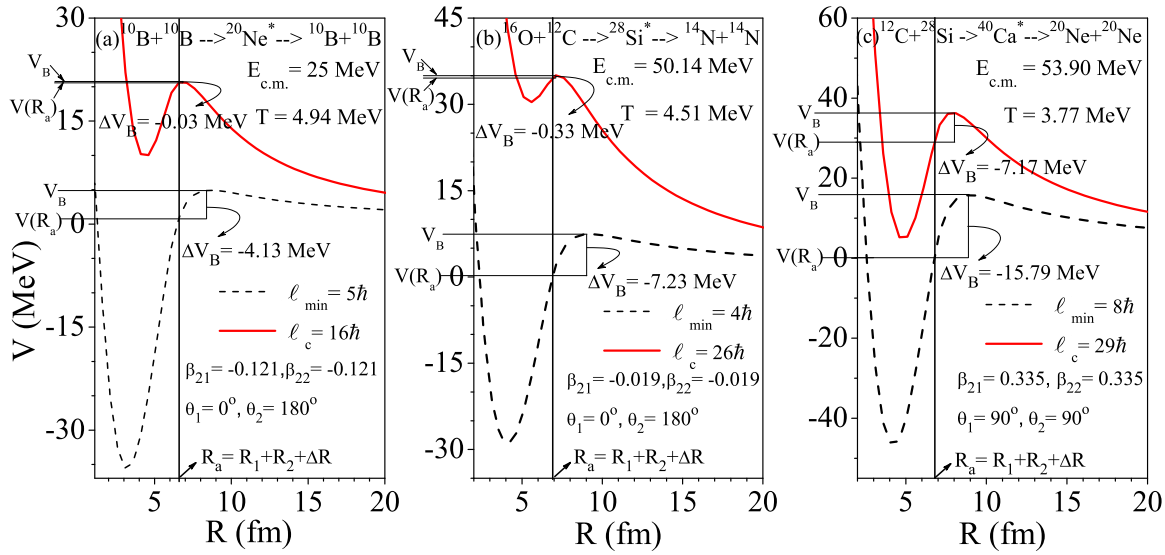

FIG. 3. Scattering potential $V(R)$ for the symmetric decay of α conjugate systems (a) ^{20}Ne*, (b) ^{28}Si*, and (c) ^{40}Ca* at $\ell_{\min}$ and respective ℓ_c values.

conjugate composite systems at different excitation energies and to compare the available experimental data [12–14] with the DCM calculations. Figure 2 presents the results for clustering effects, showing the largest preformation probability, i.e., maxima in P_0 with respect to the cluster mass ($A_i, i = 1,2$) for the decay of $N = Z$ [Fig. 2(a)] ^{20}Ne*, [Fig. 2(b)] ^{28}Si*, and $N \neq Z$ [Fig. 2(c)] ^{21}Ne*, [Fig. 2(d)] ^{22}Ne* nuclear systems. Figure 2(a) shows that, for $N = Z$, ^{20}Ne* at $T = 1.59$ MeV (with pairing constant $\delta = 32.73$ MeV), the most probable cluster configurations are $\alpha + {}^{16}$O and ^{8}Be$+{}^{12}$C. At $T = 4.94$ MeV (pairing constant $\delta = 0.77$ MeV), in addition to the most probable xα-type clusters at $T = 1.59$ MeV, np-xα-type clusters; namely, ^{6}Li, ^{10}B, and ^{14}N clusters also appear as prominent clusters. For ^{28}Si* at $T = 2.33$ MeV (with pairing constant $\delta = 31.19$ MeV), Fig. 2(b) shows that ^{4}He$+{}^{24}$Mg is the most probable cluster configuration (largest P_0), followed by the ^{8}Be$+{}^{20}$Ne and ^{12}C$+{}^{16}$O cluster configurations. At $T = 4.51$ MeV (pairing constant $\delta = 2.11$ MeV), in addition to the most probable clusters at $T = 2.33$ MeV, ^{6}Li, ^{10}B, ^{14}N, ^{18}F, and ^{22}Na (np-xα-type clusters) also appear as prominent clusters.

On the other hand, for the cases of $N \neq Z$ systems, ^{21}Ne* [Fig. 2(c)] at $T = 2.29$ MeV (with pairing constant $\delta = 31.30$ MeV), ^{4}He$+{}^{17}$O ($\equiv \alpha + n + {}^{16}$O) cluster configuration competes with ^{8}Be$+{}^{13}$C ($\equiv 2\alpha + n + {}^{12}$C) clustering. At $T = 4.67$ MeV (pairing constant $\delta = 1.53$ MeV), in addition to the most probable clusters at $T = 2.29$ MeV, ^{6,7}Li, ^{14,15}N clusters also appear as prominent clusters. For ^{22}Ne* [Fig. 2(d)] at $T = 2.59$ MeV (with pairing constant $\delta = 30.43$ MeV), ^{4}He$+{}^{18}$O ($\equiv \alpha + 2n + {}^{16}$O) cluster configuration competes with ^{8}Be$+{}^{14}$C clustering. At $T = 4.46$ MeV (pairing constant $\delta = 2.34$ MeV), in addition to the most probable clusters at $T = 2.59$ MeV, ^{10,12}B clusters also appear as prominent clusters. Quite interestingly, these results show that the QMFT supports clustering in $N = Z$ (^{20}Ne* and ^{28}Si*) and $N \neq Z$ (^{21}Ne* and ^{22}Ne*) nuclear systems at excitation energies corresponding to their respective decay threshold or resonant-state energies for the 4α, i.e., ^{16}O cluster and non-α cluster ^{14}C (for $N \neq Z$ ^{22}Ne* composite system only), given by the Ikeda diagrams [4,5], for taking into account the proper pairing strength in the temperature-dependent liquid drop energies [11,43]. Thus, we observe that the clusters remain same for ^{20}Ne*, ^{28}Si*, and ^{21}Ne* at all excitation energies as shown in Fig. 2, but for ^{22}Ne*, the clusters changes at higher excitation energy of 50.36 MeV. This happens because of the change in Z distribution with increasing temperature, as shown in Fig. 4. Figure 4 shows the variation of fragmentation potential with fragment charge Z for $A_2 = 4$ for the decay of non-α conjugate system ^{22}Ne*. At $E^* = 15.89$ MeV [with $\delta(T) = 30.43$ MeV], ^{4}He is energetically minimized while at higher experimental excitation energy $E^* = 50.36$ MeV [with $\delta(T) = 2.34$ MeV], n-rich ^{4}H is energetically minimized, and hence the corresponding heavy clusters for ^{22}Ne* in Fig. 2 are ^{18}O and ^{18}F, respectively.

Figures 5 and 6 present the clustering effects in the $N = Z$ composite systems [Figs. 5(a) and 6(a)] ^{20}Ne*, [Figs. 5(b) and 6(b)] ^{28}Si*, and [Figs. 5(c) and 6(c)] ^{40}Ca* at the higher excitation energy $E^*_{\rm CN}$ or T values, respectively, for the energetically favored potential-energy minima in the fragmentation potential V(η, T) and the largest preformation factor or maxima in the cluster preformation probability $P_0(A_i)$, at $\ell = 0$ as well as at respective ℓ_c. Surprisingly, at higher excitation energies clustering get changed drastically in these systems, due to decreasing pairing strength. Figures 2(a) and 6(a) for ^{20}Ne* system at different T values clearly demonstrate the probable binary symmetric cluster configuration with the IMF ^{10}B ($\equiv 2\alpha + p + n$) at higher T value showing the large preformation yield in comparison to at the lower T values, as observed also in the relativistic mean-field calculations for intrinsic excited states of ^{20}Ne [9], and also for the calculations within formalism of energy density functionals which clearly presents the similar kind of results for ^{20}Ne [10]. Moreover, the IMF ^{14}N ($\equiv 3\alpha + p + n$) appear as the most probable cluster followed by IMF or α clusters ^{12}C and ^{16}O

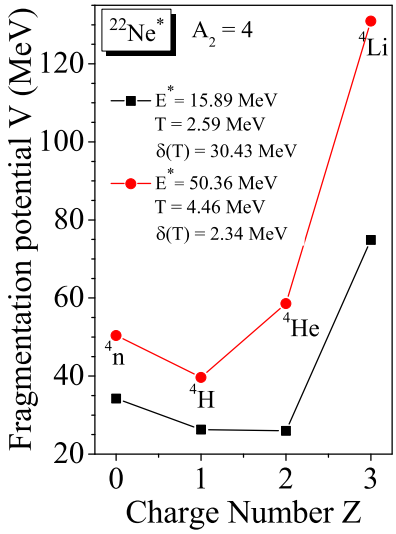

FIG. 4. Variation of the fragmentation potential V with fragment charge Z for $A_2 = 4$ fragment, for the decay of non-α conjugate system ^{22}Ne* at T values of their corresponding excited resonant state and the experimentally available excited state [13].

which are anyhow most probable at resonant state energies. Also, ^{18}F ($\equiv 4\alpha + p + n$) is in strong competition with the α clusters. Figures 2(b) and 6(b) for another $N = Z$ composite system ^{28}Si* system at different T values present the most probable binary symmetric cluster configuration with the IMF ^{14}N ($\equiv 3\alpha + p + n$) at higher T value showing the largest preformation yield in comparison to at the lower T values. The α clusters ^{16}O and ^{20}Ne, respectively, have strong competition from ^{18}F ($\equiv 4\alpha + p + n$) and ^{22}Na ($\equiv 5\alpha + p + n$). It is interesting to note that another $N = Z$ composite system ^{40}Ca* [Fig. 6(c)] also presents a similar kind of picture with binary symmetric decay (^{20}Ne) in competition with α as well as non-α clusters ($x\alpha + p + n$).

For the $N \neq Z$ composite system ^{21}Ne*, Figs. 2(c) and 7(a), at different T values, demonstrate that the ^{13}C ($\equiv 3\alpha + n$) cluster is still dominant at higher T value with competing binary near symmetric cluster configuration with the IMFs ^{10}B ($\equiv 2\alpha + p + n$) and ^{11}B ($\equiv 2\alpha + p + 2n$) and ^{17}O ($\equiv 4\alpha + n$) cluster configuration is now not favored. Other clusters or IMFs ^{14}N ($\equiv 3\alpha + p + n$) and ^{15}N ($\equiv 3\alpha + p + 2n$) are strongly competing with other new possibilities. Figures 2(d) and 7(b) for another $N \neq Z$ composite system ^{22}Ne* system at different T values present the most probable binary near-symmetric cluster configuration with the IMFs ^{10}B ($\equiv 2\alpha + p + n$) and ^{12}B ($\equiv 2\alpha + p + 3n$) at higher T value showing the largest preformation yield in comparison to ones at the lower T values. Now, the non-α cluster ^{14}C is replaced by the IMF ^{14}N ($\equiv 3\alpha + p + n$) competing strongly with the binary decay. The IMF ^{15}N ($\equiv 3\alpha + p + 2n$), ^{16}N ($\equiv 3\alpha + p + 3n$) and ^{18}F ($\equiv 4\alpha + p + n$) are also having small maxima. Note that ^{18}O ($\equiv 4\alpha + 2n$) is replaced by ^{18}F ($\equiv 4\alpha + p + n$) at higher excitation energies. Another $N \neq Z$ composite system ^{39}K* [Fig. 6(c)] presents asymmetric decay with ^{6}Li ($\equiv \alpha + p + n$) the most probable IMFs followed by ^{10}B ($\equiv 2\alpha + p + n$), ^{13}C ($\equiv 3\alpha + n$) and ^{14}N ($\equiv 3\alpha + p + n$) along with α clusters ^{12}C and ^{16}O.

Thus, at higher excitation energies, we notice from Figs. 6(a)–6(c) that, for $N = Z$ composite systems, $x\alpha$-type clusters are preformed in addition to the ($x\alpha + p + n$)-type clusters, which is due to smaller pairing strength at higher temperatures in the liquid drop energies. On the other hand, for the $N \neq Z$ composite systems we find from Figs. 7(a)–7(c) that, at higher excitation energies, ($x\alpha + xn$)- and ($x\alpha$ + p + xn)-type clusters are preformed, specifically for ^{21,22}Ne* systems, whereas for ^{39}K*, in addition, the α clusters also come into the picture. These results are of important consequences

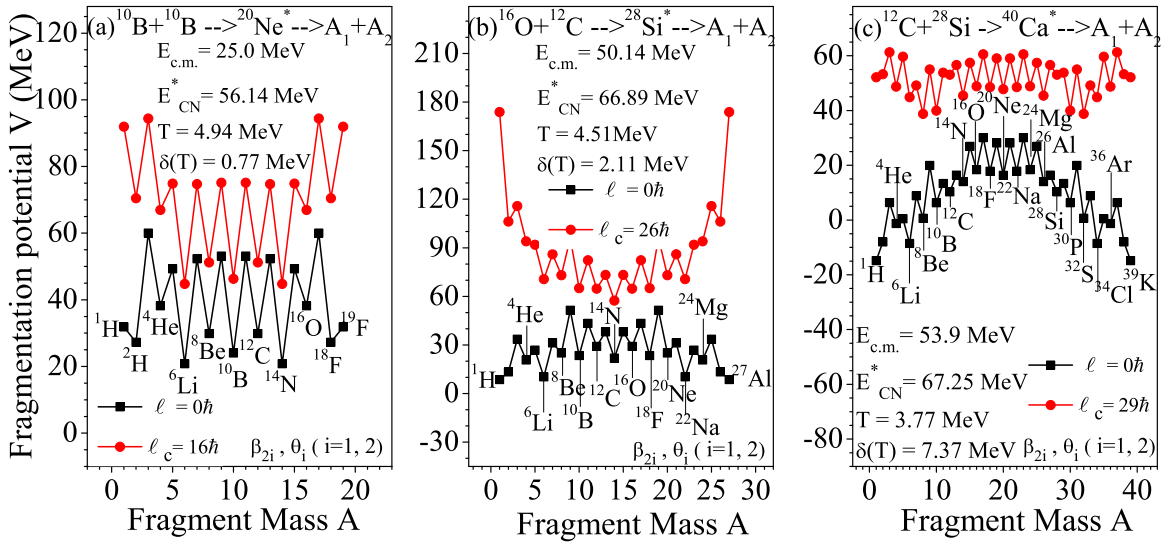

FIG. 5. Variation of fragmentation potential V with fragment mass (A_i, $i = 1,2$) for the decay of α conjugate systems (a) ^{20}Ne* (b) ^{28}Si*, and (c) ^{40}Ca* at $\ell = 0$ and respective ℓ_c values. The values of fitted ΔR for the excitation energies in the figure for ^{20}Ne* are 2.12, 2.02, 1.781 (for $Z = 5,6,7$, respectively), for ^{28}Si* they are 1.223, 1.542, 1.585 (for $Z = 3,4,5$, respectively), and for ^{40}Ca* they are 1.14, 1.14, 1.34 (for $Z = 3,4,5$, respectively); also given in Table I.

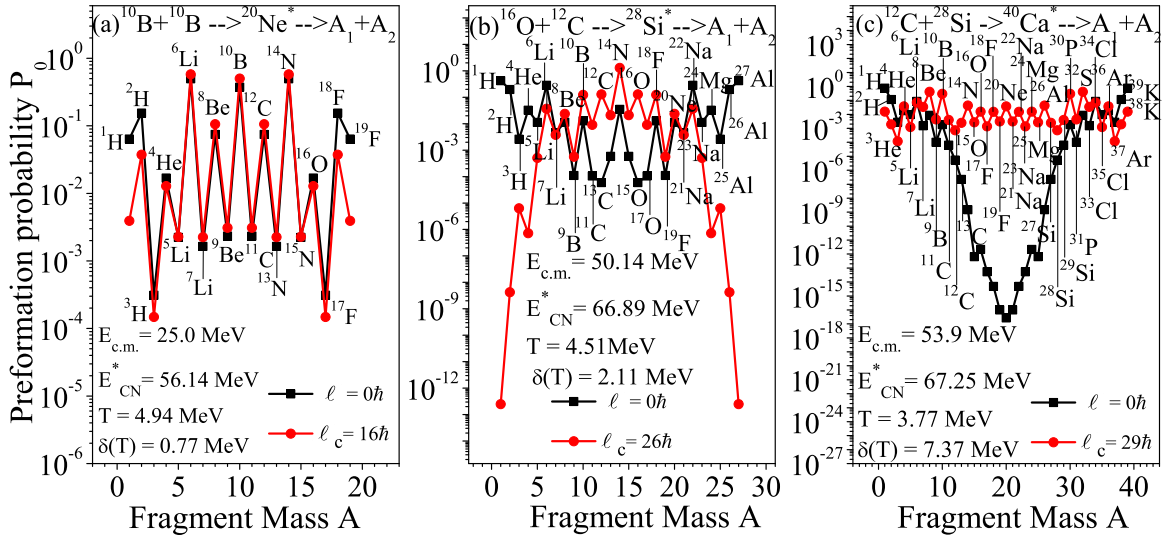

FIG. 6. Variation of preformation probability P_0 with fragment mass (A_i, $i = 1,2$) for the decay of α conjugate systems (a) ^{20}Ne*, (b) ^{28}Si*, and (c) ^{40}Ca* at $\ell = 0$ and respective ℓ_c values, calculated for fragmentation potentials in Fig. 5.

for the observed yields of IMFs having $Z = 3,4,5$ from ^{28}Si*, ^{40}Ca*, and ^{39}K* composite systems (or $Z = 7,6,5$ complimentary fragments from ^{20}Ne* and ^{21,22}Ne* composite systems) which have the experimental data available for their Z distribution.

Next, in the following, we compare the decay of $N = Z$ or α conjugate and $N \neq Z$ or non-α conjugate composite systems into the measured IMFs in terms of preformation profile of clusters or fragments, i.e., P_0, penetrability through interaction potential, i.e., P and the calculated σ_{FF}^{DCM}, followed by empirical evaluation of DIO contribution in the experimental yield, i.e., $\sigma_{DIO} = \sigma_{IMF}^{Expt} - \sigma_{FF}^{DCM}$.

Figures 5(a)–5(c) show that, in the case of ^{20}Ne* for $Z = 5,6,7$, the energetically favoured or the cluster at the minima are ^{10}B, ^{11,12}C, and ^{13,14,15}N, respectively, and in case of ^{28}Si* and ^{40}Ca* for $Z = 3,4,5$, the energetically favored clusters are ^{5,6,7}Li, ^{8}Be, and ^{9,10}B, respectively. Also, here we see that at $\ell = 0\hbar$, the LPs ($1 \leqslant A \leqslant 4$) or equivalently, evaporation residue (ER) are competing with the IMFs or clusters. At higher ℓ values, IMFs are the dominant mode of decay. As discussed earlier, at $\ell = \ell_c$, there is a strong minima for the symmetric decay of $N = Z$ (^{20}Ne* and ^{28}Si*) or α-conjugate systems. As shown in Figs. 6(a)–6(c), the energetically favored clusters are stable and thus have higher P_0. Similarly, Figs. 7(a)–7(c) present that the highly preformed

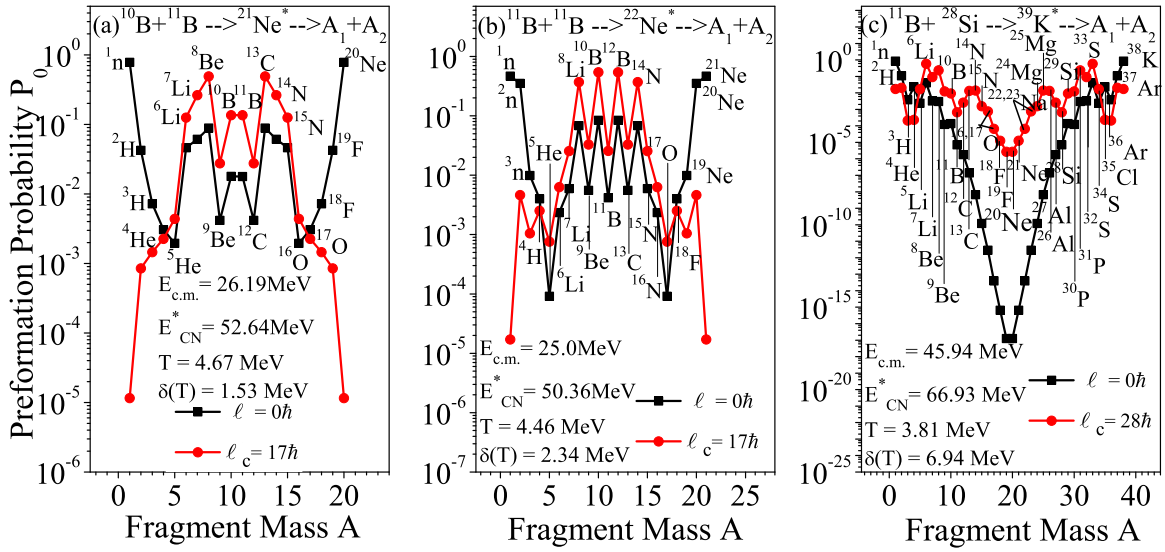

FIG. 7. Variation of preformation probability P_0 with fragment mass (A_i, $i = 1,2$) for the decay of non-α conjugate systems (a) ^{21}Ne*, (b) ^{22}Ne*, and (c) ^{39}K* at $\ell = 0$ and respective ℓ_c values. The values of fitted ΔR for the excitation energies in the figure for ^{21}Ne* are 2.0, 1.92, 1.78 (for $Z = 5,6,7$ respectively), for ^{22}Ne* they are 1.765, 2.0, 1.82 (for $Z = 5,6,7$ respectively), for ^{39}K* they are 0.97, 1.16, 1.78 (for $Z = 3,4,5$, respectively). See also Table II.

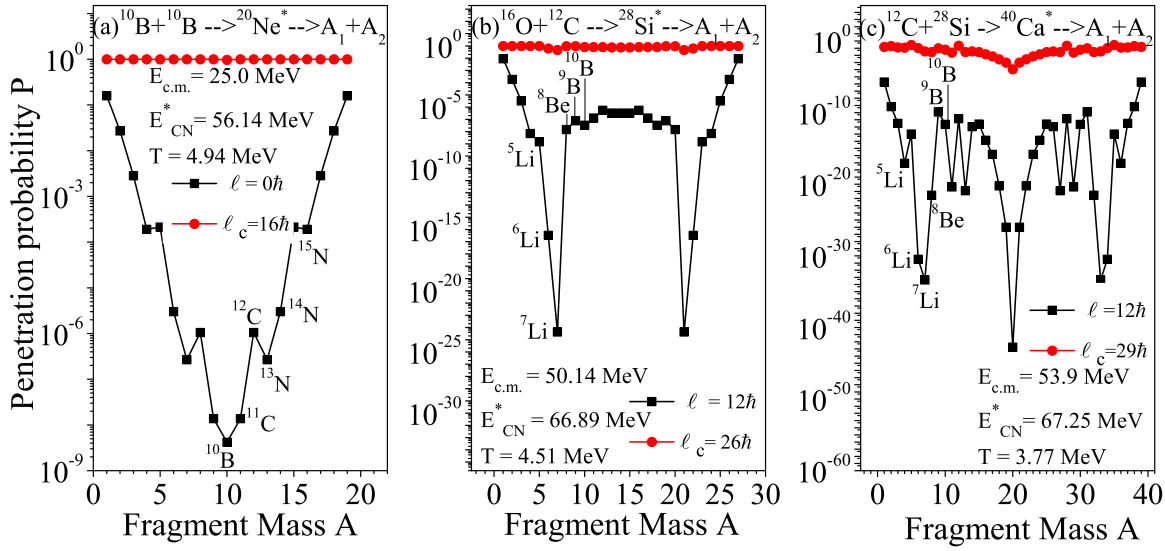

FIG. 8. Variation of penetration probability P with cluster mass (A_i, $i = 1,2$) for the decay of α conjugate systems (a) ^{20}Ne*, (b) ^{28}Si*, and (c) ^{40}Ca* at $\ell_{\min}$ and respective ℓ_c values.

clusters in the case of $N \neq Z$ composite systems ^{21}Ne* for $Z = 5,6,7$ are ^{10,11}B, ^{12,13}C, and ^{14,15}N, respectively, and in case of ^{22}Ne*, for $Z = 5,6,7$ are ^{10,11}B, ^{13}C, and ^{14,15,16}N, respectively, and in case of ^{39}K*, for $Z = 3,4,5$, are ^{5,6,7}Li, ^{8,9}Be, and ^{10,11}B, respectively.

Figures 8(a)–8(c) depict the penetration of different IMFs or clusters for $N = Z$ composite systems and, in general, we see that their $P \to 1$ at $\ell = \ell_c$, while at low angular momentum in the case of ^{20}Ne* [Fig. 8(a)], the ^{10}B cluster has the smallest P while it is preformed strongly and ^{11,12}C and ^{13,14,15}N have the higher value of P. In the case of ^{28}Si* [Fig. 8(b)], at low angular momentum, the ^{7}Li has the smallest P and other clusters ^{5,6}Li, ^{8}Be, ^{9,10}B have higher P. In the case of ^{40}Ca* [Fig. 8(c)] also, at low angular momentum, the ^{7}Li has a smaller P value in comparison to ^{5,6}Li, ^{8}Be, and ^{9,10}B, whereas the ^{20}Ne cluster has the smallest P although it has a high value of P_0. Figures 9(a)–9(c) present a similar kind of picture but for the $N \neq Z$ composite systems, with the exception that of ^{39}K* [Fig. 9(c)], the symmetric fragments have very high P values contrary to their low P_0 values.

Following the above results, the calculations for $\sigma_{\rm FF}^{\rm DCM}$ and their comparisons with $\sigma_{\rm IMF}^{\rm Expt}$ for the $N = Z$ and $N \neq Z$ composite systems are presented, respectively, in Tables I and II. The empirically evaluated $\sigma_{\rm DIO}$ are also presented here for ^{20,21,22}Ne* and ^{28}Si* systems. Note that the experimental data are fit by adjusting the neck-length parameter (ΔR) simultaneously within the proximity range. Table I shows that, in the case of ^{20}Ne*, $Z = 5$, ^{10}B has the highest P_0 but has smallest penetrability P (see Figs. 6 and 8) which is in line with the experimental cross section ($\sigma_{\rm IMF}^{\rm Expt}$) which is least for $Z = 5$

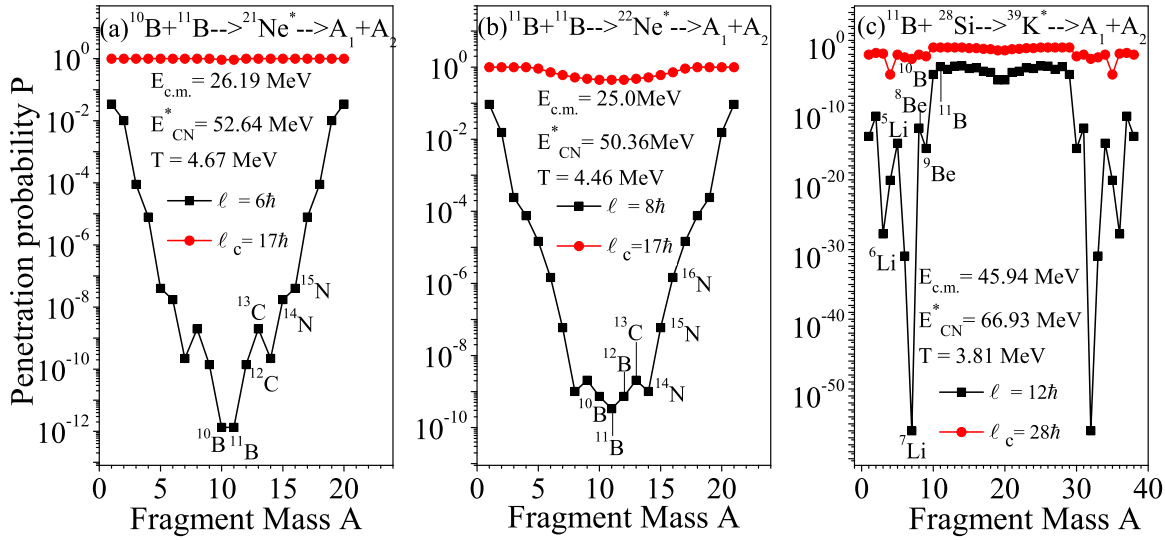

FIG. 9. Variation of penetration probability P with cluster mass (A_i, $i = 1,2$) for the decay of non-α conjugate systems (a)^{21}Ne, (b) ^{22}Ne*, and (c) ^{39}K* at $\ell_{\min}$ and respective ℓ_c values.

TABLE I. The DCM-calculated FF cross sections σ_{FF}^{DCM} for the decay of $^{20}Ne^*$, $^{28}Si^*$ and $^{40}Ca^*$ summed up to ℓ_c, and the σ_{DIO} estimated empirically and compared with experimental data.

$E_{c.m.}$	E^*_{CN}	T	ℓ_c	ΔR (fm)			σ_{FF}^{DCM} (mb)			σ_{IMF}^{Expt} (mb)			σ_{DIO}^{emp} (mb)		
(MeV)	(MeV)	(MeV)	($\hbar$)	$Z=5$	$Z=6$	$Z=7$	$Z=5$	$Z=6$	$Z=7$	$Z=5$	$Z=6$	$Z=7$	$Z=5$	$Z=6$	$Z=7$
$^{10}B + {}^{10}B \rightarrow {}^{20}Ne^*$															
12	43.14	4.35	12	2.118	2.2	2.171	77.37	48.33	312.73	77.37	192.90	313.25		144.57	
15	46.14	4.50	13	2.13	2.2	2.14	115.56	57.45	337.98	115.01	427.10	482.41		369.65	144.43
20	51.14	4.72	15	2.112	2.10	1.9	214.69	70.75	275.18	214.33	376.40	334.83		305.65	59.65
24	55.14	4.90	16	2.1	2.0	1.8	254.56	62.13	234.79	268.70	472.06	247.33	14.14	409.93	12.54
25	56.14	4.94	16	2.12	2.02	1.781	252.42	60.89	205.72	303.0	510.75	205.33	50.58	449.86	
$E_{c.m.}$	E^*_{CN}	T	ℓ_c	ΔR (fm)			σ_{FF}^{DCM} (mb)			σ_{IMF}^{Expt} (mb)			σ_{DIO}^{emp} (mb)		
(MeV)	(MeV)	(MeV)	($\hbar$)	$Z=3$	$Z=4$	$Z=5$	$Z=3$	$Z=4$	$Z=5$	$Z=3$	$Z=4$	$Z=5$	$Z=3$	$Z=4$	$Z=5$
$^{16}O + {}^{12}C \rightarrow {}^{28}Si^*$															
50.14	66.89	4.51	26	1.223	1.542	1.585	17.06	12.72	38.34	42.68	14.20	60.28	25.62	1.48	21.94
53.57	70.32	4.62	26	1.24	1.56	1.61	16.79	11.86	37.38	44.12	17.32	63.95	27.33	5.46	26.57
62.14	78.89	4.92	26	1.31	1.625	1.67	16.56	10.98	34.24	68.34	21.53	83.31	51.78	10.55	49.07
68.57	85.32	5.08	25	1.47	1.75	1.792	20.36	11.58	32.02	95.16	33.13	126.48	74.80	21.55	94.46
$E_{c.m.}$	E^*_{CN}	T	ℓ_c	ΔR (fm)			σ_{FF}^{DCM} (mb)			σ_{FF}^{Expt} (mb)					
(MeV)	(MeV)	MeV)	($\hbar$)	$Z=3$	$Z=4$	$Z=5$	$Z=3$	$Z=4$	$Z=5$	$Z=3$	$Z=4$	$Z=5$			
$^{12}C + {}^{28}Si \rightarrow {}^{40}Ca^*$															
53.90	67.20	3.77	29	1.14	1.14	1.34	4.08	2.81	3.82	$3.7^{+5.4}_{-1.7}$	$2.7^{+4.1}_{-1.2}$	$3.4^{+5.1}_{-1.5}$			

among $Z = 5,6,7$. For $Z = 5$, the decay mode is FF while the DIO comes into picture at two higher energies. For $Z = 7$, the dominant decay mode is FF at the lowest energy and at higher energies DIO is present. The percent-age contribution of DIO is maximum near the entrance channel, i.e., $Z = 6$. In the case of $^{28}Si^*$, for $Z = 4$ the percent-age FF contribution is comparatively more than in $Z = 3,5$ clusters. There is an enhanced yield near the entrance channel, i.e., $Z = 5$. For $Z = 3$, the percent-age DIO is greater and increases with increasing energy. For $^{40}Ca^*$, the FF cross sections are well reproduced for $Z = 3,4,5$ and are compared with experimental data.

TABLE II. The DCM-calculated FF cross sections σ_{FF}^{DCM} for the decay of $^{21}Ne^*$, $^{22}Ne^*$, and $^{39}K^*$ summed up to ℓ_c value, and the σ_{DIO} estimated empirically and compared with experimental data.

$E_{c.m.}$	E^*_{CN}	T	ℓ_c	ΔR (fm)			σ_{FF}^{DCM} (mb)			σ_{IMF}^{Expt} (mb)			σ_{DIO}^{emp} (mb)		
(MeV)	(MeV)	(MeV)	($\hbar$)	$Z=5$	$Z=6$	$Z=7$	$Z=5$	$Z=6$	$Z=7$	$Z=5$	$Z=6$	$Z=7$	$Z=5$	$Z=6$	$Z=7$
$^{10}B + {}^{11}B \rightarrow {}^{21}Ne^*$															
13.09	39.54	4.07	12	1.987	2.2	2.2	17.29	142.15	171.92	17.36	802.48	600.83		660.33	428.91
15.71	42.16	4.20	13	2.09	2.2	2.2	45.85	183.10	219.05	46.31	739.95	732.66		556.85	513.16
20.95	47.40	4.44	15	2.19	2.12	2.05	111.86	241.13	201.36	111.16	881.22	743.16		640.09	541.80
26.19	52.64	4.67	17	2.0	1.92	1.78	109.28	231.53	168.24	159.80	713.31	484.10	50.52	481.78	315.86
$^{11}B + {}^{11}B \rightarrow {}^{22}Ne^*$															
12	37.36	3.87	12	1.75	2.2	2.2	3.93	13.82	80.86	3.99	288.33	80.43		274.81	
15	40.36	4.02	14	1.782	2.2	2.11	30.29	25.12	166.86	30.26	378.54	166.30		353.42	
20	45.36	4.25	15	1.86	2.2	2.02	61.17	19.46	142.56	61.09	493.31	220.10		473.85	77.54
24	49.36	4.42	17	1.73	1.96	1.81	82.14	14.91	130.49	82.21	537.27	298.91		522.36	168.42
25	50.36	4.46	17	1.765	2.0	1.82	88.70	15.16	124.63	88.49	560.68	410.86		545.32	286.23
$E_{c.m.}$	E^*_{CN}	T	ℓ_c	ΔR (fm)			σ_{FF}^{DCM} (mb)			σ_{FF}^{Expt} (mb)					
(MeV)	(MeV)	MeV)	($\hbar$)	$Z=3$	$Z=4$	$Z=5$	$Z=3$	$Z=4$	$Z=5$	$Z=3$	$Z=4$	$Z=5$			
$^{11}B + {}^{28}Si \rightarrow {}^{39}K^*$															
45.94	66.93	3.81	28	1.11	1.33	1.936	9.20	6.23	2.96	$8.5^{+10.0}_{-5.8}$	$5.3^{+8.0}_{-2.3}$	$21.0^{+32.1}_{-9.2}$			
$^{12}C + {}^{27}Al \rightarrow {}^{39}K^*$															
50.53	67.14	3.81	30	0.97	1.16	1.78	9.30	5.06	2.53	$8.5^{+10.6}_{-6.2}$	$4.2^{+5.8}_{-3.0}$	$9.^{+13.0}_{-5.2}$			

Table II shows that, in the case of ^{21}Ne*, $Z = 5$ ^{10,11}B are preformed strongly having competition with ^{8}Be and ^{13}C but have the least penetrability (see Figs. 7 and 9) which is in line with the experimental cross section ($\sigma_{\rm IMF}^{\rm Expt}$) which is least for $Z = 5$ among $Z = 5,6,7$. For $Z = 5$, the decay mode is FF while the DIO comes into the picture at the highest energy. In the case of $Z = 6$, ^{13}C has the highest P_0 and good penetrability P (see Figs. 7 and 9) and has the highest experimental cross section among $Z = 5,6,7$. For $Z = 6,7$, the dominant decay mode is DIO which increases with increasing energy. In the case of ^{22}Ne*, for $Z = 5$ the $\sigma_{\rm IMF}^{\rm Expt}$ is the smallest in comparison with $Z = 6,7$. Also, the results within the DCM show that the symmetric breakup into ^{11}B is least favored in terms of P_0 and P (refer to Figs. 7 and 9) and the FF is the only decay mode at all experimental energies (for $Z = 5$). For $Z = 6$ (i.e., near to the entrance channel), the DIO is the significant decay mode. For ^{39}K*, the FF cross sections are well reproduced for $Z = 3,4$ while for $Z = 5$ we are not able to obtain a good agreement with experimental data. The percent contribution of FF is more in α composite systems in comparison with non-α composite systems. The results, within the DCM, are in good agreement with the experimental data.

IV. SUMMARY

The clustering effects in the light-mass $N = Z$ (^{20}Ne*, ^{28}Si*, and ^{40}Ca*) and $N \neq Z$ (^{21,22}Ne* and ^{39}K*) composite systems, with considerations of quadrupole deformations and compact orientations of nuclei, have been studied within the QMFT-based DCM and their comparative decay analysis undertaken. The calculations at $T = 0$ and corresponding to excitation energies near to decay threshold given by Ikeda diagram, by taking into account the temperature-dependent pairing-energy term in liquid drop energies reveal that, in $N = Z$ nuclear systems, $x\alpha$-type (where x is an integer) cluster configurations are dominant while in $N \neq Z$ nuclear systems, xn-$x\alpha$-type cluster configurations are dominant. These results are in conformity with cluster configurations given by the Ikeda diagram. However, the clustering scenario at experimentally available excitation energies is changed due to decreasing pairing strength at high energies. In addition to $x\alpha$ configuration in $N = Z$ composite systems and xn-$x\alpha$-type configuration in $N \neq Z$ composite systems, the np-$x\alpha$-type configurations are having comparatively higher preformation probability in these systems.

Thus, the present study explores the role of nuclear structure effects via preformation probability P_0, which enters the collision dynamics within the formalism of DCM. The emission of different intermediate mass fragments or clusters with $Z = 3,4,5$ (or complementary fragments $Z = 5,6,7$ in ^{20,21,22}Ne*) have also been studied in terms of fragmentation potential V, preformation probability P_0, and penetration P through the interaction potential and IMF cross section by fitting the only parameter (i.e., neck length parameter) within the proximity range, in reference to available Z-distribution data. The study shows the coexistence of competing reaction mechanisms, i.e., FF and DIO in the decay of light-mass composite systems under study. The contribution of DIO in total cross section of IMFs has been evaluated empirically. The percent contribution of FF is more in $N = Z$ (α conjugate) systems in comparison to $N \neq Z$ (non-α conjugate) systems. The calculated cross sections, using the DCM, are in good agreement with experimental data.

ACKNOWLEDGMENTS

B.B.S. acknowledges the support from the Department of Science and Technology (DST), New Delhi, in the form of a Young Scientist Award under the SERC Fast Track Scheme, vide letter No. SR/FTP/PS-013/2011. B.B.S. and M.K. are highly thankful to the Theoretical Nuclear Physics Group at Institute of Physics (IOP), Bhubaneswar, for the fruitful discussions related to the research and the kind hospitality during their stay at IOP for the part of present research work.

[1] G. Gamow, Eur. Phys. J. A **51**, 204 (1928).
[2] F. Hoyle, D. N. F Dunbar, W. A. Wenzel, and W. Whaling, Phys. Rev. **92**, 1095c (1953), Minutes of the New Mexico Meeting, Alberquerque, September 2–5.
[3] C. W. Cook, W. A. Fowler, and T. Lauritsen, Phys. Rev. **107**, 508 (1957).
[4] L. R. Hafstad and E. Teller, Phys. Rev. **54**, 681 (1938); K. Ikeda, N. Takigawa, and H. Horiuchi, Prog. Theor. Phys. Suppl. **E68**, 464 (1968).
[5] W. Von Oertzen *et al.*, Eur. Phys. J. A **11**, 403 (2001); W. Von Oertzen, M. Freer, and Y. Kanada-Enyo, Phys. Rep. **432**, 43 (2006); W. Von Oertzen *et al.*, Eur. Phys. J. A **43**, 17 (2010).
[6] R. K. Sheline and K. Wildermuth, Nucl. Phys. **21**, 196 (1960); F. D. Becchetti, K. T. Hecht, J. Janecke, and D. Overway, Nucl. Phys. A **339**, 132 (1980); D. Jenkins, J. Phys. Conf. Series **436**, 012016 (2013).
[7] G. V. Rogachev *et al.*, Prog. Theor. Phys. Suppl. **196**, 184 (2012); J. Phys.: Conf. Ser. **569**, 012004 (2014).
[8] T. Yahmaya, Phys. Lett. B **306**, 1 (1993); M. Freer and A. C. Merchant, J. Phys. G **23**, 261 (1997); G. V. Rogachev, V. Z. Goldberg, T. Lönnroth, W. H. Trzaska, S. A. Fayans, K. M. Källman, J. J. Kölata, M. Mutterer, M. V. Rozhkov, and B. B. Skorodumov, Phys. Rev. C **64**, 051302(R) (2001); M. Freer, Rep. Prog. Phys. **70**, 2149 (2007); E. D. Johnson *et al.*, Eur. Phys. J. A **42**, 135 (2009); J. A. Scarpaci, M. Fallot, D. Lacroix, M. Assie, L. Lefebvre, N. Frascaria, D. Beaumel, C. Bhar, Y. Blumenfeld, A. Chbihi, P. Chomaz, P. Desesquelles, J. Frankland, H. Idbarkach, E. Khan, J. L. Laville, E. Plagnol, E. C. Pollacco, P. Roussel-Chomaz, J. C. Roynette, A. Shrivastava, and T. Zerguerras, Phys. Rev. C **82**, 031301(R) (2010).
[9] P. Arumugam, B. K. Sharma, S. K. Patra, and R. K. Gupta, Phys. Rev. C **71**, 064308 (2005).
[10] J. P. Ebran, E. Khan, T. Niksic, and D. Vretenar, Nature (London) **487**, 341 (2012); Phys. Rev. C **87**, 044307 (2013); **89**, 031303(R) (2014).
[11] M. Bansal, R. Kumar, and R. K. Gupta, J. Phys.: Conf. Ser. **321**, 012046 (2011).
[12] A. Szanto de Toledo *et al.*, Phys. Rev. Lett. **62**, 1255 (1989).
[13] M. M. Coimbra *et al.*, Nucl. Phys. A **535**, 161 (1991).

[14] S. Kundu, C. Bhattacharya, K. Banerjee, T. K. Rana, S. Bhattacharya, A. Dey, T. K. Ghosh, G. Mukherjee, J. K. Meena, P. Mali, S. Mukhopadhyay, D. Pandit, H. Pai, S. R. Banerjee, D. Gupta, P. Banerjee, S. Kumar, A. Shrivastava, A. Chatterjee, K. Ramachandran, K. Mahata, S. K. Pandit, and S. Santra, Phys. Rev. C **85**, 064607 (2012); S. Kundu, Parmana **82**, 727 (2014).
[15] S. Kundu, A. Dey, K. Banerjee, T. K. Rana, S. Muhkopadhayay *et al.*, Phys. Rev. C **78**, 044601 (2008).
[16] A. Dey, C. Bhattacharya, S. Bhattacharya, S. Kundu, K. Banerjee *et al.*, Phys. Rev. C **76**, 034608 (2007).
[17] K. Daneshvar, D. G. Kovar, S. J. Krieger, and K. T. R. Davies, Phys. Rev. C **25**, 1342 (1982).
[18] D. Shapira, R. Novotny, Y. D. Chan, K. A. Erb, and J. L. C. Ford Jr., Phys. Lett. B **114**, 111 (1982).
[19] C. Beck, Y. Abe, N. Aissaoui, B. Djerroud, and F. Hass, Nucl. Phys. A **583**, 269 (1995); Phys. Rev. C **49**, 2618 (1994).
[20] S. J. Sanders, Phys. Rev. C **44**, 2676 (1991); C. Beck, *ibid.* **53**, 1989 (1996).
[21] C. Beck, B. Djerroud, F. Haas, R. M. Freeman, A. Hachem *et al.*, Phys. Rev. C **47**, 2093 (1993).
[22] K. A. Farrar, S. J. Sanders, A. K. Dummer, A. T. Hasan, F. W. Prosser *et al.*, Phys. Rev. C **54**, 1249 (1996).
[23] B. B. Singh, G. Kaur, M. K. Sharma, and R. K. Gupta, Proc. DAE Symp. **56**, 474 (2011); **57**, 550 (2012); B. B. Singh, P. Kumar, S. Kanwar, and R. K. Gupta, *ibid.* **58**, 380 (2013), http://www.sympnp.org/proceedings/; B. B. Singh, M. Kaur, M. K. Sharma, and R. K. Gupta, J. Phys.: Conf. Ser. **569**, 012030 (2014); EPJ Web Conf. **86**, 00049 (2015).
[24] S. S. Malik, S. Singh, R. K. Puri, S. Kumar, and R. K. Gupta, Pramana **32**, 419 (1989).
[25] G. Kaur and M. K. Sharma, Int. J. Mod. Phys. E **23**, 1450063 (2014).
[26] B. B. Singh, M. K. Sharma, R. K. Gupta, and W. Greiner, Int. J. Mod. Phys. E **15**, 699 (2006).
[27] R. K. Gupta, M. Balasubramaniam, R. Kumar, D. Singh, C. Beck, and W. Greiner, Phys. Rev. C **71**, 014601 (2005).
[28] S. K. Arun, R. K. Gupta, B. B. Singh, S. Kanwar, and M. K. Sharma, Phys. Rev. C **79**, 064616 (2009); **80**, 034317 (2009).
[29] B. B. Singh, M. Kaur, V. Kaur, and R. K. Gupta, EPJ Web Conf. **86**, 00048 (2015); B. B. Singh, M. Kaur, and R. K. Gupta, JPS Conf. Proc **6**, 030001 (2015).
[30] R. K. Gupta, M. Balasubramaniam, R. Kumar, N. Singh, M. Manhas *et al.*, J. Phys. G **31**, 631 (2005).
[31] R. K. Gupta, M. Manhas, and W. Greiner, Phys. Rev. C **73**, 054307 (2006).
[32] J. Marhun and W. Greiner, Phys. Rev. Lett. **32**, 548 (1974).
[33] H. J. Fink, J. Marhun, W. Scheid, and W. Greiner, Eur. Phys. J. A **268**, 321 (1974).
[34] R. K. Gupta, W. Scheid, and W. Greiner, Phys. Rev. Lett. **35**, 353 (1975).
[35] R. K. Gupta, R. Kumar, N. K. Dhiman, M. Balasubramaniam, W. Scheid, and C. Beck, Phys. Rev. C **68**, 014610 (2003).
[36] B. B. Singh, M. K. Sharma, and R. K. Gupta, Phys. Rev. C **77**, 054613 (2008).
[37] H. Kröger and W. Scheid, J. Phys. G: Nucl. Phys. **6**, L85 (1980).
[38] W. D. Myers and W. D. Swiatecki, Nucl. Phys. **81**, 1 (1966).
[39] N. J. Davidson, S. S. Hsiao, J. Markram, H. G. Miller, and Y. Tzeng, Nucl. Phys. A **570**, 61c (1994).
[40] P. A. Seeger, Nucl. Phys. **25**, 1 (1961).
[41] G. Audi and A. H. Wapstra, Nucl. Phys. A **595**, 409 (1995); G. Audi, A. H. Wapstra, and C. Thiboult, *ibid.* **729**, 337 (2003).
[42] P. Möller, J. R. Nix, W. D. Myers, and W. J. Swiatecki, At. Data Nucl. Data Tables **59**, 185 (1995).
[43] R. K. Gupta, S. K. Arun, R. Kumar, and Niyti, Int. Rev. Phys. (IREPHY) **2**, 369 (2008).
[44] R. K. Gupta, N. Singh, and M. Manhas, Phys. Rev. C **70**, 034608 (2004).
[45] S. S. Malik and R. K. Gupta, Phys. Rev. C **39**, 1992 (1989).